Deconvolution of Wide Field-of-View Radiometer Measurements of Earth-Emitted Radiation. Part I: Theory

G. LOUIS SMITH AND RICHARD N. GREEN

NASA Langley Research Center, Hampton, VA 23665

(Manuscript received 29 April 1980, in final form 21 October 1980)

ABSTRACT

The problem of relating satellite measurements from wide field-of-view (WFOV) radiometers to the radiant exitance emitted from the top of the atmosphere is treated. The problem is formulated as an integral equation to be solved for the radiant exitance distribution in terms of the measurements. An analytical solution to this integral equation in terms of spherical harmonics is presented for the case in which the directional dependence of the outgoing radiation is a function of zenith angle only. It is shown that the resolution which can be obtained under real conditions is limited.

The sensitivity of the derived radiant exitance distribution to the directional dependence of the outgoing radiation is studied, and results are presented for WFOV flat-plate and spherical radiometers and for restricted field-of-view flat-plate radiometers. It is demonstrated that this sensitivity is a function of the scale of spatial resolution; thus higher resolutions in the radiant exitance distribution are more sensitive to variations in the directional dependence.

The technique is applied to measurements of earth-emitted radiation from the Nimbus 6 ERB (Earth Radiation Budget) experiment WFOV radiometer to produce a resolution enhanced map of emitted radiation for the month of August 1975. For this case, the limit of resolution appeared to be spherical harmonics of degree 15. Comparison with results from the ERB scanning radiometer shows very good agreement.

1. Introduction

The theory of deconvolution of wide field-of-view (WFOV) radiometer measurements of earth-emitted radiation is presented. This theory provides a technique by which the resolution of such measurements can be enhanced to provide radiant exitance at the top of the atmosphere with a finer resolution than the field of view.

There are two major classes of radiometers: wide field-of-view radiometers, which receive radiation from horizon to horizon and scanning radiometers, which measure radiation within a relatively small solid angle at any instant and which move this narrow field of view through some scan pattern. The scanner with its narrow field of view provides far more resolution, hence more information, than does the WFOV radiometer. However, this resolution is gained at the expense of signal-to-noise ratio and the complexity of the scanning mechanisms. Also, the scan patterns in practice omit many directions of incoming radiation.

The use of satellite radiometers to measure the earth radiation budget was demonstrated by Suomi (1960) with hemispherical sensors aboard the Explorer 7 spacecraft. With increasing complexity of spacecraft permitting more refined instrumentation, the scanning medium-resolution infrared radiometer aboard the Nimbus 3 spacecraft provided a wealth of radiation budget data (Raschke *et al.*, 1973).

The most sophisticated experiment to date for measurement of radiation budget is the Earth Radiation Budget (ERB) experiment which first flew aboard the Nimbus 6 spacecraft in June 1975 (Smith *et al.*, 1977; Jacobowitz *et al.*, 1979). This experiment included a set of wide-field-of-view radiometers, a bidirectional scanner with four longwave and four shortwave channels, and 10 solar channels. The scanner provided valuable data from July 1975, when the instrument was turned on, until October 1975, when it was turned off because of malfunction. The WFOV channels and solar channels, however, have continued to function well and have provided four years of data thus far. Another ERB experiment was flown in October 1978 aboard the Nimbus 7 spacecraft and is providing data.

The next satellite experiment which is planned for measuring radiation budget is the Earth Radiation Budget Experiment (ERBE), which is scheduled to be launched in the mid-1980's.[1] Like the ERB, the ERBE includes both wide field-of-view and scanning radiometers, as well as solar radiometers.

[1] Woerner, C. V., 1978: The earth radiation budget satellite system: An overview. *Preprints Third Conf. Atmospheric Radiation*, Davis, Amer. Meteor. Soc., 345–348.

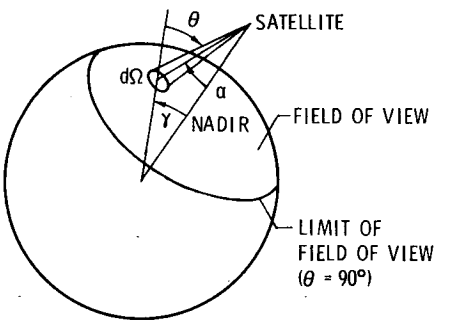

FIG. 1. Wide field-of-view radiometer data analysis problem.

The nature of the wide-field-of-view problem is illustrated in Fig. 1. The unrestricted field of view at the Nimbus 6 altitude of 1100 km is a circle on the earth's surface with a diameter of over 60° of great circle arc. Each data point is an integral of the irradiance from all points within the field of view, weighted by the directional response of the sensor. Given global coverage using a flat-plate-type radiometer (i.e., one with a cosine response), it is conceptually straightforward to extract the globally integrated emitted heat flux from such a set of measurements. The originally intended use of WFOV data was for heat flux measurements at very large scales. However, information on a finer scale than the total field of view is desirable.

The problem of deconvolving a set of WFOV radiometer measurements to obtain radiant exitance at a finer resolution than the instantaneous field of view has been treated previously, beginning with House.[2] In essence, the measurement is an integral of the radiance from portions of the earth within the field of view, which is related to the radiant exitance at the top of the atmosphere by use of radiation directional models. The computation of radiant exitance is thus formulated as the solution of an integral equation. Pina and House[3] have treated this problem by partitioning the earth's surface into regions of uniform radiant exitance, so that the integral equation is reduced to a set of simultaneous linear algebraic equations. Also, they considered the weighted least-squares solution of the problem with an abundance of data; i.e., an overdetermined system. Smith and Green[4] demonstrated that for the axisymmetric case with a simple radiation directional model, the eigenfunctions of the measurement integral operator are Legendre polynomials, which permits an analytic solution to the integral equation. In that paper, it was demonstrated analytically that the high spatial frequency components of data errors would be amplified by the deconvolution process. This effect limits the resolution which is obtainable. A technique was developed by Pina and House for stabilizing the measurement matrix, whereby small terms in the measurement matrix are added to the largest terms in their respective rows and equated to zero in their original positions.

In the present paper, an analytical solution for the earth-emitted radiant exitance in terms of WFOV radiometer measurements is derived for the nonaxisymmetric (or regional) case, in which the measurements and radiant exitance are considered to be functions of both latitude and longitude. This solution makes it possible to deconvolve a set of WFOV radiometer measurements of earth-emitted radiation and obtain information with a finer resolution than the instantaneous field of view of the instrument. However, there are limits to the level of resolution which can be achieved in this manner; these limits are coarser than those obtainable with scanning radiometers. Interpretation of both WFOV and scanning radiometer data requires knowledge of the directional characteristics of the earth-atmosphere system. It is shown that there are tradeoffs involved in the selection between WFOV and scanning radiometers. The criteria which form the basis for these tradeoffs include accuracy at a given level of resolution. This analysis is not applicable to the interpretation of reflected exitance.

This is Part I of a set of two papers. In Part II, Bess *et al.* (1981) apply this theory to one year of Nimbus 6 ERB wide-field-of-view earth-emitted data in order to interpret the data with the maximum obtainable resolution.

2. Notation

b_j^n	coefficient in spherical harmonic expansion of radiant exitance M (W m^{-2})
$d^j_{mn}(\Theta_s)$	rotation term defined by Eq. (A3)
D^j_{mn}	rotation matrices for spherical harmonics
$g(\alpha)$	angular response of sensor
h	altitude of satellite (km)
L	radiance (W m^{-2} sr^{-1})
$\mathcal{L}$	measurement operator [see Eqs. (4) and (11)]
m	measurement (W m^{-2})
$M(\Theta,\Phi)$	radiant exitance at top of atmosphere (W m^{-2})
N	degree of spherical harmonic expansion, beyond which series is truncated
$P_j(x)$	Legendre polynomial of order j

[2] House, F. B., 1972: Deconvolution of wide-field radiative measurements from satellites. Presented at *Conf. Atmospheric Radiation,* Fort Collins, Amer. Meteor. Soc.

[3] Pina, J. F., and F. B. House, 1975: An inversion method for computing radiances and albedos of earth-atmosphere regions from wide-angle satellite sensor measurements. *Preprints Second Conf. Atmospheric Radiation,* Arlington, Amer. Meteor. Soc., 119–122.

[4] Smith, G. Louis, and Richard N. Green, 1975: A technique for analysis of low resolution measurements of earth radiation budget. *Preprints Second Conf. Atmospheric Radiation*, Arlington, Amer. Meteor. Soc., 111–114.

r	distance from satellite to point on earth's surface
r	position vector
r_e	radius of earth (6378.165 km)
$R(\theta)$	limb-darkening function
x, y, z	geocentric Cartesian coordinate system
$Y_j^n(\Theta,\Phi)$	spherical harmonic of degree j and order n
α	cone angle from satellite nadir to point on surface of earth (see Fig. 1)
α_r	aperture angle for restricted-field-of-view sensor
α_h	cone angle from satellite nadir to horizon
β	clock angle; i.e., azimuthal angle at subsatellite point between north and great circle arc to surface element on earth
γ	geocentric angle between satellite and earth surface element
Θ	colatitude
θ	zenith angle
λ_j	jth eigenvalue of measurement operator
σ_j	degree variance
Φ	longitude
Ω	solid angle, steradians
ω	function defined by Eq. (21)

Subscripts

alt	altitude of satellite
lam	Lambertian
nom	nominal
s	satellite.
toa	top of atmosphere

3. Analysis

a. Assumptions

In order to obtain an analytic solution for the deconvolution of wide field-of-view radiometer measurements of earth-emitted radiation, the following four simplifying assumptions are made:

(i) The sensor integrates incoming radiation over its field of view, with its directional response a function only of nadir angle.

(ii) The directional dependence of exiting radiation at each point at the top of the atmosphere is a function only of the zenith angle of the exiting ray.

(iii) Continuous measurements are available over a sphere concentric with the earth.

(iv) The measurement field at spacecraft altitude is sampled in such a way as to produce a good estimate of the time average of the field, and the radiometer response is time invariant.

Assumption (i) is applicable to most WFOV sensors due to their design. An interesting special case for which this assumption is applicable is a nadir oriented radiometer with an iris restricting the field of view. Assumption (ii) is a reasonable approximation for earth-emitted radiation, but not suited for reflected solar radiation. Assumption (iii) contains two requirements. The first requirement is that continuous measurements be available over a surface, which is a frequent mathematical demand, incompatible with a physical system providing discrete measurements, and usually worked around. The second requirement is that the orbit be circular. These requirements can be alleviated by using an approach such as that presented by Smith, Green and Campbell (1975)[5] by which the problem is treated as a statistical problem of parameter estimation. The mathematical structure which is discussed in the present paper underlies the parameter estimation solution.

Assumption (iv) permits us to relate the mean measurement field to the mean flux field. Because time-averaged quantities are dealt with, time does not appear in this formulation. Statistical problems due to temporal variability and a finite sample set are beyond the scope of the present paper.

b. Formulation of problem

A wide-field-of-view radiometer at satellite altitude is considered. The relevant geometry is shown in Fig. 2. The earth-atmosphere system will be approximated by a sphere of radius r_e. The radiation leaving any point on the surface of the sphere is dependent on both position and direction. The radiation will be assumed to be a function of colatitude Θ and of longitude Φ. It will also be assumed to be a function of zenith angle, and independent of azimuth. The radiance from a surface element may be written

$$L(\Theta,\Phi,\theta) = \pi^{-1}M(\Theta,\Phi)R(\theta), \qquad (1)$$

where $R(\theta)$ is the limb-darkening function which is assumed to be independent of position and indicates the angular distribution of the observed surface brightness. Note that reflected exitance is a function of solar zenith angle; because this variable is not included in the formulation, this analysis is applicable to emitted radiation and not to reflected radiation. For a Lambertian radiator, $R(\theta) = 1$. The radiant exitance is also related to the radiance $L(\Theta,\Phi,\theta)$ by

$$M(\Theta,\Phi) = \int_{2\pi} L(\Theta,\Phi,\theta)\cos\theta d\Omega, \qquad (2)$$

where $d\Omega$ is the differential of solid angle. From Eqs. (1) and (2), it follows that $R(\theta)$ satisfies the

[5] Smith, G. Louis, Richard N. Green, and G. G. Campbell, 1975: A statistical interpretation technique for wide angle radiometer measurements of earth energy. *Preprints Fourth Conf. Probability and Statistics in Atmospheric Science*, Tallahassee, Amer. Meteor. Soc., 171–176.

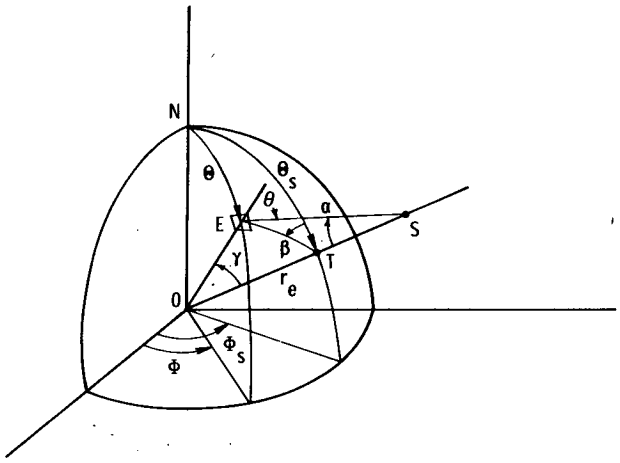

FIG. 2. Satellite-earth geometry.

equation

$$2\int_0^{\pi/2} R(\theta)\cos\theta\sin\theta d\theta = 1. \quad (3)$$

Thus, the limb-darkening function is normalized by this condition rather than by the convention that $R(0) = 1$ which is often used.

The measurement due to radiation from the earth incident on the sensor at a colatitude Θ_s and longitude Φ_s is

$$m(\Theta_s,\Phi_s) = \int_\Omega L(\Theta,\Phi,\theta)g(\alpha)d\Omega$$
$$= \frac{1'}{\pi}\int_\Omega M(\Theta,\Phi)R(\theta)g(\alpha)d\Omega$$
$$= \frac{1}{\pi}\int_{\beta=0}^{\beta=2\pi}\int_{\alpha=0}^{\alpha=\alpha_h} M(\Theta,\Phi)R(\theta)g(\alpha) \times \sin\alpha d\alpha d\beta, \quad (4)$$

where $g(\alpha)$ is the angular response of the sensor to incoming radiation and α_h is the cone angle from satellite nadir to horizon. For a spherical sensor $g(\alpha) = 1$, and for a black flat plate, $g(\alpha) = \cos\alpha$. Surface properties for other type sensors can be incorporated in $g(\alpha)$ provided the angular response is dependent only on the nadir angle and independent of the azimuthal angle. The angles Θ, Φ and θ can be expressed in terms of the cone and clock angles, α and β, and the colatitude and longitude of the sensor, Θ_s and Φ_s.

From the geometry of Fig. 2, it may be shown that

$$\theta = \gamma + \alpha, \quad (5)$$

$$\cos\Theta = \cos\Theta_s/\sin\alpha_h - (\cos\Theta_s\cos\alpha - \sin\Theta_s\sin\alpha\cos\beta)r/r_e, \quad (6)$$

$$\sin(\Phi_s - \Phi) = \sin\gamma\sin\beta/\sin\Theta, \quad (7)$$

$$\sin\gamma = (r\sin\alpha)/r_e, \quad (8)$$

$$r/r_e = [\cos\alpha - (\sin^2\alpha_h - \sin^2\alpha)^{1/2}]/\sin\alpha_h, \quad (9)$$

$$\sin\alpha_h = r_e/(r_e + h). \quad (10)$$

Eqs. (5)–(10) express θ, Θ, and Φ in terms of the satellite position (Θ_s,Φ_s) and the variables of integration (α,β). Thus, Eq. (4) is the desired relationship between the measured radiation $m(\Theta_s,\Phi_s)$ and the unknown radiant exitance $M(\Theta,\Phi)$. This relationship may be conveniently written as

$$m(\Theta_s,\Phi_s) = \mathcal{L}M(\Theta,\Phi), \quad (11)$$

where $\mathcal{L}$ denotes the linear integral operator and $R(\theta)$ and $g(\alpha)$ are included in the kernal function.

c. *Solution of integral equation*

The problem is now stated as follows: Assuming that measurements m are given over an entire sphere of radius r_e surrounding the earth and the kernel of $\mathcal{L}$ is known, what is the radiant exitance $M(\Theta,\Phi)$ leaving the top of the atmosphere? With $m(\Theta_s,\Phi_s)$ specified over the entire sphere, it is possible to solve the integral Eq. (11) for $M(\Theta,\Phi)$.

The solution of the integral Eq. (11) is facilitated by noting that the eigenfunctions of the operator $\mathcal{L}$ are spherical harmonics, i.e.,

$$\mathcal{L}Y_j^n(\Theta,\Phi) = \lambda_j Y_j^n(\Theta_s,\Phi_s). \quad (12)$$

This is a consequence of the invariance of the operator $\mathcal{L}$ with position over the earth and with rotation about the nadir line, and is demonstrated in Appendix A. Furthermore, the eigenvalues are shown to be given by

$$\lambda_j = 2\int_0^{\alpha_h} P_j(\cos\gamma)R(\theta)g(\alpha)\sin\alpha d\alpha. \quad (13)$$

With the use of Eq. (12), the solution of Eq. (11) now proceeds as follows.

If $M(\Theta,\Phi)$ is a piecewise continuous function over the globe, then it can be expanded in a series of spherical harmonics, which form a complete set

$$M(\Theta,\Phi) = \sum_{j=0}^{\infty}\sum_{n=-j}^{j} b_j^n Y_j^n(\Theta,\Phi). \quad (14)$$

The measurement $m(\Theta_s,\Phi_s)$ is then, by use of Eqs. (11), (12), and (14)

$$m(\Theta_s,\Phi_s) = \sum_{j=0}^{\infty}\sum_{n=-j}^{j} b_j^n \mathcal{L}Y_j^n(\Theta,\Phi)$$
$$= \sum_{j=0}^{\infty}\sum_{n=-j}^{j} \lambda_j b_j^n Y_j^n(\Theta_s,\Phi_s). \quad (15)$$

The coefficients on the right-hand side of Eq. (15) may be determined by use of the orthogonality of the spherical harmonics, yielding

$$\frac{1}{4\pi}\int_{\Phi_s=0}^{2\pi}\int_{\Theta_s=0}^{\pi} m(\Theta_s,\Phi_s)Y_j^{n*}(\Theta_s,\Phi_s) \times \sin\Theta_s d\Theta_s d\Phi_s = \lambda_j b_j^n, \quad (16)$$

where the asterisk indicates the complex conjugate. This result is substituted into Eq. (14) to give the radiant exitance at the top of the earth-atmosphere system in terms of the wide-field-of-view measurements at altitude:

$$M(\Theta,\Phi) = \sum_{j=0}^{N}\sum_{n=-j}^{j}\frac{1}{\lambda_j}Y_j^n(\Theta,\Phi) \times \frac{1}{4\pi}\int_{\Phi_s=0}^{2\pi}\int_{\Theta_s=0}^{\pi} m(\Theta_s,\Phi_s)Y_j^{n*}(\Theta_s,\Phi_s) \times \sin\Theta_s d\Theta_s d\Phi_s. \quad (17)$$

As will be discussed, the problem is ill-posed and the summation over j must be terminated at some finite N, rather than summed to infinity. Eq. (17) may be written in the form

$$M(\mathbf{r}) = \int_{\Phi_s=0}^{2\pi}\int_{\Theta_s=0}^{\pi} G(\mathbf{r},\mathbf{r}_s)m(\mathbf{r}_s)\sin\Theta_s d\Theta_s d\Phi_s, \quad (18)$$

where the Green's function $G(\mathbf{r},\mathbf{r}_s)$ is given by

$$G(\mathbf{r},\mathbf{r}_s) = \sum_{n=0}^{N}\sum_{m=-n}^{n}\lambda_n^{-1}Y_n^m(\mathbf{r})Y_n^{m*}(\mathbf{r}_s). \quad (19)$$

By use of the addition theorem for spherical harmonics, Eq. (19) may be written as

$$G(\gamma) = \frac{1}{4\pi}\sum_{n=0}^{N}(2n+1)\lambda_n^{-1}P_n(\cos\gamma), \quad (20)$$

where γ denotes the geocentric angle between $\mathbf{r}$ and $\mathbf{r}_s$. Eq. (17) shows that within the framework of the four assumptions stated initially, the solution to the data inversion is simply to resolve the spherical harmonic components of the measurements, weight them by $1/\lambda_j$, and reassemble them to produce the radiant exitance at the top of the earth-atmosphere system. The sensor may be considered abstractly to be an operator which transforms the radiant exitance field into the measurements. Because of the rotational symmetry of the problem resulting from the first two assumptions, the eigenfunctions of this operator are spherical harmonics. Thus, resolution of a field into spherical harmonics is the canonical transformation appropriate to any remote sensors satisfying assumptions (i) and (ii). The correspondence of the axisymmetric problem on a sphere with a similar problem on the real line is discussed in Appendix B. The measurement operator for reflected solar radiation does not possess the rotational invariance over the sphere; hence, the present solution in terms of spherical harmonics does not apply to that problem.

For the axisymmetric case, the integrals vanish for $n \neq 0$, leaving only the $Y_j^0(\Theta,\Phi)$ terms; i.e., essentially Legendre polynomials in $\cos\Theta$, in a single summation. The first term in the series is a constant, and is simply the global mean radiation. The coefficient of the $Y_1^0(\Theta,\Phi)$ term is a large part of the pole-to-pole gradient; it is the first moment of M about the equator, thus providing a measurement of asymmetry of the radiation from the Northern and Southern Hemispheres. Likewise, the coefficient of the $Y_2^0(\Theta,\Phi)$ term is the major part of the equator-to-pole variation of radiation. This term, when computed for net radiation, is the major driving force for atmospheric and oceanic circulation.

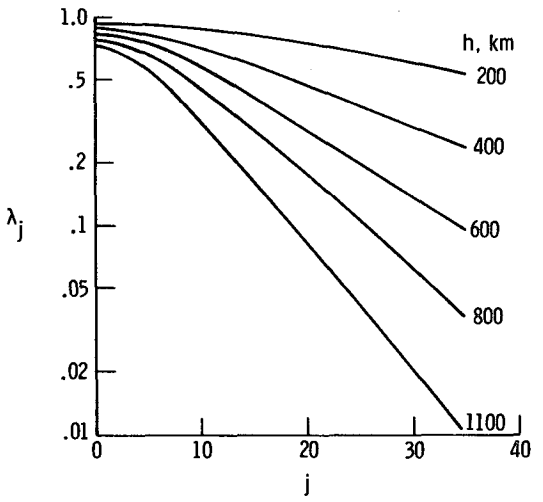

FIG. 3. Eigenvalues of measurement operator for a WFOV flat plate sensor for various measurement altitudes.

d. Behavior of eigenvalues and sensor resolution

The angular response of the sensor $g(\alpha)$ and the radiation model $R(\theta)$ determine the eigenvalues λ_j, as seen in Eq. (13). It may be demonstrated that the eigenvalues converge to zero by considering the function

$$\omega(\gamma) = \begin{cases} 2R(\theta)g(\alpha)d(\cos\alpha)/ \\ \qquad d(\cos\gamma), & 0 \leq \gamma < \gamma_h \\ 0, & \gamma \geq \gamma_h. \end{cases} \quad (21)$$

The coefficients of $\omega(\gamma)$ in a Legendre expansion are $(2j+1)\lambda_j/2$. If $R(\theta)$ and $g(\alpha)$ are well behaved, so that $\omega(\gamma)$ is well behaved, then these coefficients must form a sequence which converges to zero, and the sequence of λ_j must vanish more rapidly than $1/j$.

Fig. 3 shows the variation of λ_j with j for a number of altitudes for a flat-plate sensor, characterized by $g(\alpha) = \cos\alpha$. Also, for Fig. 3, it is assumed that $R(\theta) = 1$; i.e., that the earth is a diffuse but non-uniform radiator. The λ_0 value is the shape factor for radiative transfer to an infinitesimally small, flat plate

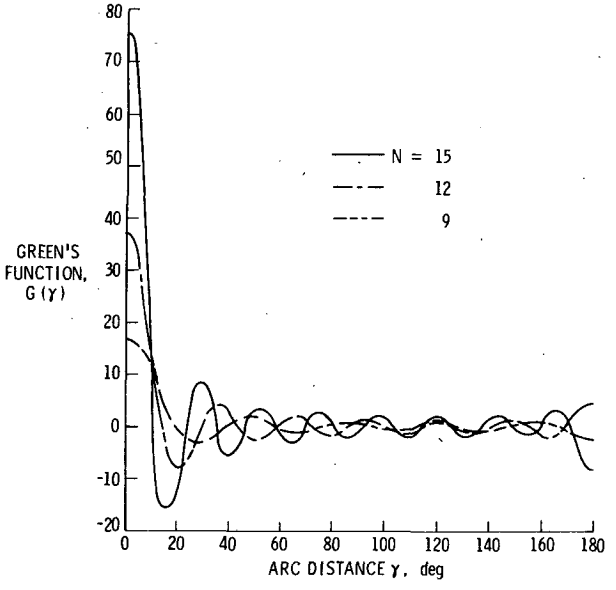

FIG. 4. Green's function for radiant exitance solution; satellite altitude = 1100 km for summation limit N = 9, 12 and 15.

from a sphere. As j increases from 0, λ_j decreases slowly initially, then decreases approximately exponentially as j becomes still larger. It is seen that as the sensor altitude increases, the slope of the λ_j curve steepens.

The decrease of λ_j as j increases may be interpreted in view of Eqs. (14) and (15). For large j, the contributions of $Y_j^n(\Theta,\Phi)$ terms to the measurement m are attenuated by the factor λ_j. These terms represent the fine-scale variation of the radiant exitance field $M(\Theta,\Phi)$, and are smoothed out by the measurement. In the data inversion process, represented by Eq. (17), fine-scale structure in the measurement field $m(\Theta_s,\Phi_s)$ is amplified by the factor $1/\lambda_j$, which grows exponentially. For perfect measurements the solution is exact; however, a small change in m can result in large changes in M, so that small errors in m result in M being dominated by high-frequency components. The problem is ill-posed, but this may be handled by terminating the series at some value $j = N$, which restricts the fineness of resolution of M which can be obtained. Physically, this means that the resolution obtainable from a set of WFOV measurements is limited by the variability of the field during the sampling period and by the accuracy of the measurements. This problem is characteristic of the analysis of remotely sensed data, and is discussed by Twomey (1965) for the general class of integral operators with smoothing kernels. In the present case, the eigenfunctions of the operator are known to be spherical harmonics and the eigenvalues are easily computed. The degree j corresponds to the number of wave node lines of the spherical harmonic $Y_j^n(\Theta,\Phi)$; as such, it is a measure of resolution of the representation. For example, including terms through the 15th degree in $Y_j^n(\Theta,\Phi)$, where $0 \leq j \leq 15$, is considered the equivalent to 12° resolution (180° pole-to-pole expressed by 15 waves), or ~1300 km. The non-axisymmetric variation is accounted for by the various orders $-j < n < j$. Thus, the discussion of resolution obtainable from data from a sensor is based on the variation of λ_j with j.

As the summation limit N in Eq. (17) increases, the correspondence of the derived M field with the true M field improves, until the error in the added terms exceeds the true magnitude of the added terms. At this point, the error incurred by including the terms of this degree is greater than the error incurred by omitting them. Thus, it is desirable to select N to be one less than this degree. At present, the selection of N is based on inspection of the data, as will be discussed in the results section.

The Green's function $G(\gamma)$ for a WFOV radiometer at altitude of 1100 km is shown in Fig. 4 for summation limit N of 9, 12 and 15. A diffuse earth is assumed in this figure. It is seen that $G(\gamma)$ has a central peak at $\gamma = 0$ and has a damped wave behavior as γ increases. As the summation limit N increases, the height of the curve increases considerably, and the width of the central peak decreases. At the antipode ($\gamma = 180°$) there is a spurious peak or dip for N even or odd, respectively. This feature is a type of Gibb's phenomenon, and becomes narrower and of higher absolute value as N increases. Fig. 5 shows the Green's function for $N = 15$ for altitudes of 600 and 1100 km. It is seen that the main effect of altitude on Green's function is to increase the ampli-

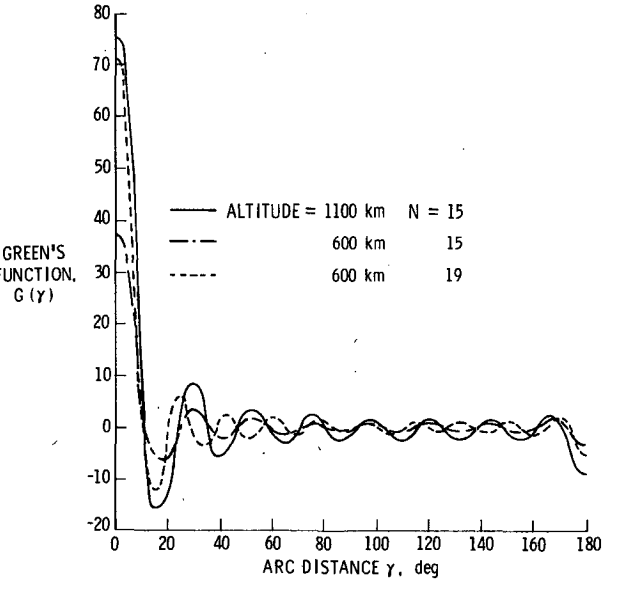

FIG. 5. Green's function for radiant exitance solution; satellite altitude = 600 and 1100 km.

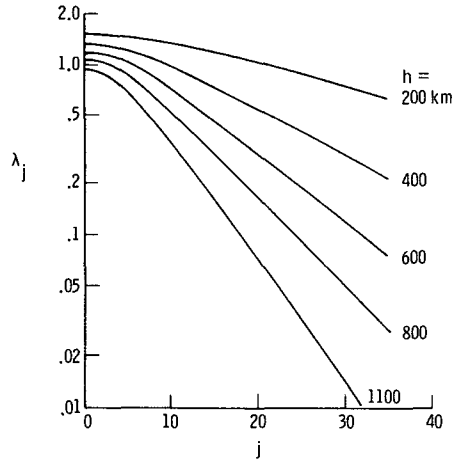

FIG. 6. Eigenvalues of measurement operator for a sphere for various measurement altitudes.

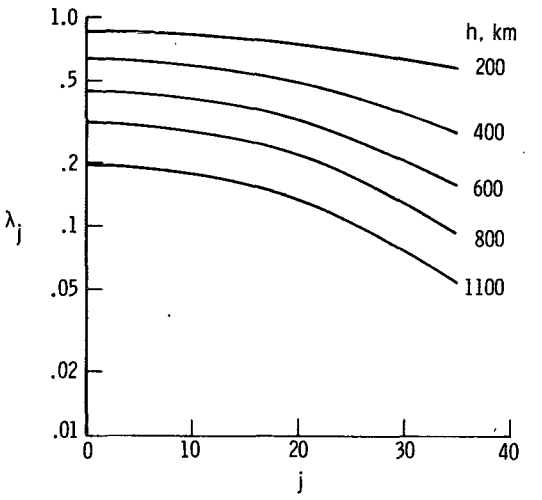

FIG. 7. Eigenvalues of measurement operator for a RFOV flat-plate sensor with field of view restricted to a circle with radius of 5° great circle arc, for various sensor altitudes.

tude of the damped wave for constant solution degree. Rather than hold the solution degree N constant in studying the effect of altitude on Green's function, one may hold the peak value approximately constant. Thus, in decreasing the altitude from 1100 to 600 km, the solution degree may be increased from 15 to 19. It is seen from Fig. 5 that the resulting Green's function has a higher frequency and damps more rapidly as γ increases. Obviously, if one decreases the measurement altitude to the top of the atmosphere, the measurement becomes the desired radiant exitance and the Green's function becomes the Dirac delta function.

e. Application to sensor selection

As was discussed in the previous section, the behavior of the eigenvalues is a factor in determining the resolution available from the radiometers, and the eigenvalues of flat-plate-type radiometers were discussed. It is also of interest to consider other types of sensors. In this section, the eigenvalues of restricted field of view and spherical radiometers will be examined. Also, the sensitivity of the eigenvalues to changes in the limb-darkening function will be investigated.

The eigenvalues of the measurement operator for a spherical sensor [$g(\alpha) = 1$] are shown in Fig. 6 for various measurement altitudes. For small j, the spherical sensor has larger λ_j than does the flat plate (Fig. 3) because it receives more radiation from large nadir angles. For large j, the λ_j values decrease more rapidly due to stronger cancellation effects of the $P_j(\cos\gamma)$ at large nadir angles. Consequently, the spherical sensor will provide lower resolution than will the flat plate.

One concept of interest is a nadir-viewing flat-plate radiometer with a circular aperture restricting the field of view. The present analysis is applicable to the restricted-field-of-view (RFOV) sensor by defining

$$g(\alpha) = \begin{cases} \cos\alpha, & 0 \leq \alpha < \alpha_r \\ 0, & \alpha > \alpha_r, \end{cases}$$

where α_r is the nadir angle beyond which the view is shielded by the aperture. The aperture angle α_r is determined by the size of the field of view on the earth's surface desired, which is measured in terms of Earth central angle γ_r. The eigenvalues for RFOV sensors are shown in Figs. 7 and 8 for Earth central angles of 5 and 10°, respectively, for various altitudes. When comparing Figs. 7 and 8 with Fig. 3, it may be seen that for altitudes > 400 km, λ_j decreases with increasing j much more slowly for the RFOV sensor than for the WFOV sensor. This simply indicates that the resolution for the RFOV sensor is

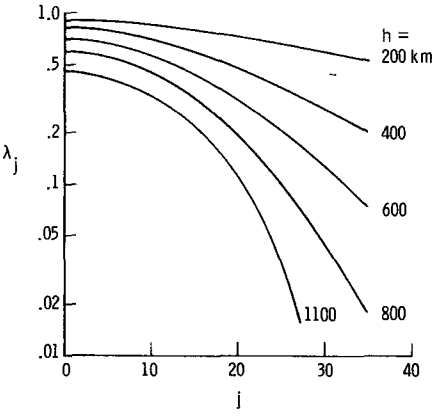

FIG. 8. Eigenvalues of measurement operator for a RFOV flat-plate sensor with field of view restricted to a circle with radius of 10° great circle arc, for various sensor altitudes.

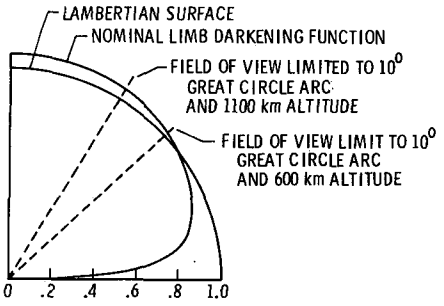

FIG. 9. Polar plot of variation of directional model with zenith angle for nominal limb-darkening function and Lambertian surface.

finer than for the flat plate. Below 400 km, the aperture does not limit the field of view much, so the eigenvalues for the RFOV sensors are very nearly the same as for the WFOV flat plate.

The sensitivity of the derived radiant exitance M at the top of the atmosphere to the directional dependence is of concern in radiometer selection and design, as the directional dependence cannot be known accurately at each position and time. It is thus desirable to select the radiometer which is least sensitive to these errors for a given level of resolution. This sensitivity to directional error is studied by assuming that M is computed from Eq. (17) on the basis of Lambertian emission, as well as on the basis of a realistic limb-darkening function. Such a computation provides an upper bound for the error due to uncertainties or variations of the limb-darkening function. A nominal directional dependence function representing a crude average of the limb-darkening functions used by Raschke *et al.* (1973) is shown in Fig. 9. This curve can be approximated by

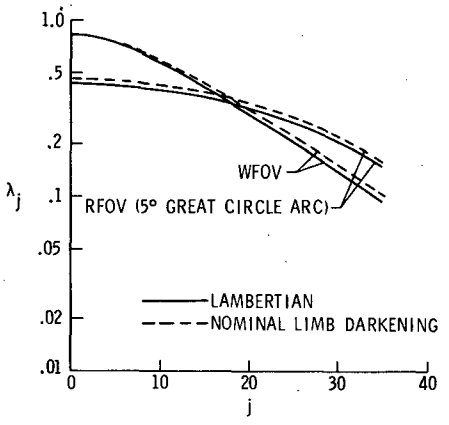

FIG. 10. Eigenvalues of wide field-of-view and restricted field-of-view sensors for Lambertian and limb-darkening directional functions. Altitude = 600 km.

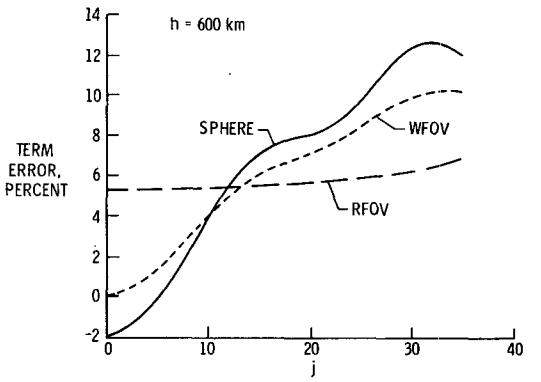

FIG. 11. Term errors due to data interpretation using Lambertian assumption with limb-darkening present for satellite altitude of 600 km.

$$R(\theta) = \begin{cases} 1.074 \exp\left[0.106\left(1 - \dfrac{1}{\cos\theta}\right)\right], \\ \qquad 0° \leq \theta < 60° \\ 1.074 \exp\left[-0.056 + 0.05 \right. \\ \qquad \left. \times \left(1 - \dfrac{1}{\cos\theta}\right)\right], \quad 60° \leq \theta \leq 90°. \end{cases} \tag{22}$$

This function has been normalized so as to satisfy Eq. (3).

Fig. 10 shows a comparison of the eigenvalues for a Lambertian earth-atmosphere system [$R(\theta) = 1$] and for nominal limb darkening, as computed from Eq. (13). Results are shown for both a flat-plate sensor and a restricted-field-of-view (RFOV) sensor which has a field-of-view radius of 5° great circle arc at the top of the atmosphere, which is taken to be 30 km altitude for this study. It is seen that the eigenvalues are modified somewhat by limb darkening, but their general behavior is not changed.

The percentage error in each term for the $M(\Theta,\Phi)$ computation is

$$\epsilon_j = \left(\frac{\lambda_{j,\text{nom}}}{\lambda_{j,\text{lam}}} - 1\right) \times 100. \tag{23}$$

This error is shown in Fig. 11 for 600 km altitude and in Fig. 12 for 1100 km altitude for WFOV flat-plate, RFOV flat-plate and WFOV spherical sensors. It is seen that the WFOV flat plate has no modeling error at the global scale, $j = 0$. This may be demonstrated by a change of variables in Eq. (13) from α to θ, whereby the integral reduces to the normalizing condition of Eq. (3) multiplying an inverse square of distance. This result also may be demonstrated in a more general manner by considering conservation of radiant energy between the top of the atmosphere and a control surface at orbital al-

titude. Furthermore, this result is unique to a sensor with unrestricted field of view having a $\cos\alpha$ response; i.e., a flat-plate or equivalent type radiometer. For this reason, the λ_j curves as shown in Fig. 10 merge at $j = 0$ for the WFOV flat-plate sensor. As j increases, the term error increases considerably, and comparison of Figs. 11 and 12 shows increasing sensitivity with altitude. A spherical sensor shows similar behavior for large j, but for $j = 0$ the sensor is sensitive to directional model errors.

The RFOV sensor is seen in Figs. 11 and 12 to have a nearly constant error over a large range of j. This appears in Fig. 10 as a nearly constant displacement of the eigenvalues for the RFOV sensor. For lower altitude, the field of view of the RFOV sensor for 10° great circle arc resolution is less restricted, so that the sensor behaves more as a flat plate and has less error. These considerations are brought out by noting the portion of the angular distribution which is viewed by the 10° great circle arc RFOV sensor, as indicated in Fig. 9. As the altitude of the sensor increases, the portion of the angular distribution which is viewed decreases.

4. Application to measurements

Measurements of earth-emitted radiation for August 1975 from the WFOV channels of the ERB instrument aboard the Nimbus 6 spacecraft (Jacobowitz, 1979) have been deconvolved by use of Eq. (17). The algorithm used for implementing this computation used 5° × 5° GARP type "quasi-square" boxes as a grid system. Data points within each box were averaged, and the $m(\mathbf{r}_s)$ was assumed constant over each box in order to evaluate the area integral in Eq. (17). The resulting spherical harmonic coefficients serve as a vector representation of the field. It was found that the field is dominated by the axisymmetric terms for $j = 0$ to 4. A useful condensation of the coefficients is the degree variance σ_j^2, which provides a measure of the spatial spectrum of a field over a globe, and is defined by

$$\sigma_j^2 = \sum_{i=-j}^{i} b_j^i b_j^{i*}.$$

The degree variance in shown as a function of degree j in Fig. 13 for the measured radiant exitance field as measured at the satellite and as inferred at the top of the atmosphere. The two spectra are related by

$$\sigma_j^2(\text{toa}) = \lambda_j^{-2}\sigma_j^2(\text{alt}),$$

where the λ_j associated with a Lambertian assumption are used and the sensor is assumed to have a flat-plate response. It is seen that the radiant exitance spectrum as measured at satellite altitude divides into two regions: one in which $\log\sigma_j^2(\text{alt})$ decreases linearly with j for $j \leq 15$, and the other in which $\log\sigma_j^2(\text{alt})$ is rather constant for $j > 15$.

The measured field has variations on it due to fluctuations of the radiation field during the month, discretization errors imposed during the analysis, and instrument errors. For comparison, the spectrum of a simulated random field at satellite altitude is shown in Fig. 13. This spectrum was generated by assigning a random number from a normal distribution with mean zero and standard deviation 10 W m^{-2} to each grid box. The simulation approximated the equivalent of white noise on a sphere, for which the variances of spherical harmonic coefficients are equal for all degrees and orders (Heiskanen and Moritz, 1967). The degree variance σ_j^2 for such a process then varies as $(2j + 1)$, which is indicated by the dashed line. It is seen that the simulation follows the theoretical curve out to degree 18, beyond which the degree variance of the simulated noise appears constant through degree 36. For the

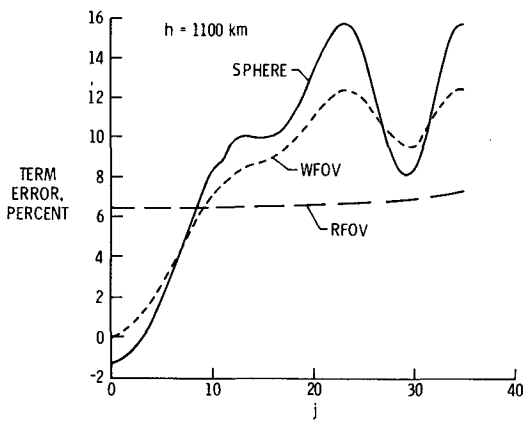

FIG. 12. Term errors due to data interpretation using Lambertian assumption with limb-darkening present for satellite altitude of 1100 km.

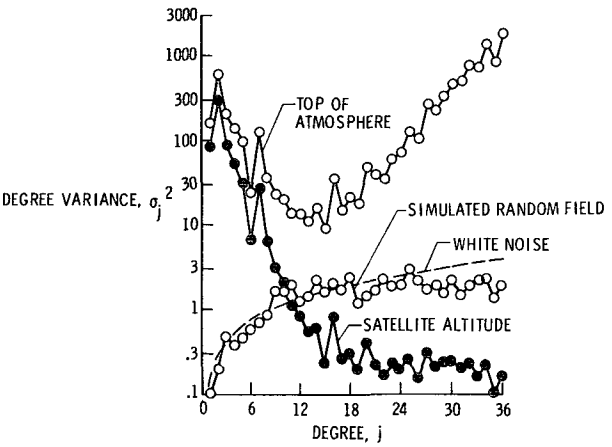

FIG. 13. Earth radiant exitance spatial spectrum, August 1975.

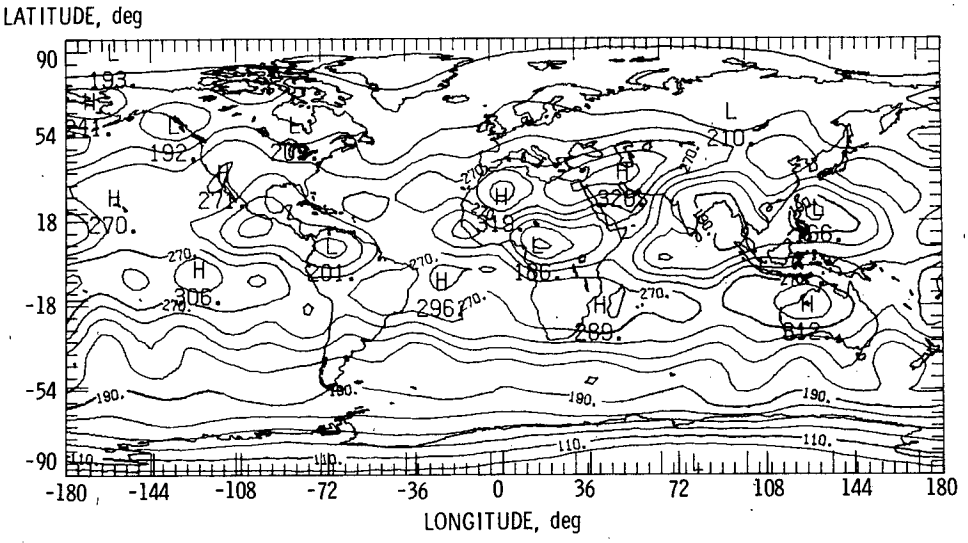

FIG. 14. Map of longwave radiant exitance at top of atmosphere for August 1975.

simulation, the noise in effect is perfectly correlated over each 5° × 5° grid box, although the boxes are uncorrelated from each other. Thus, for high degrees, the resolution of the grid system reduces the degree variance of a random field below that of a white noise field. This effect of grid system on spherical harmonic coefficients extracted from data has been studied, for example, by Rapp (1977). In the present case it is concluded that the constant degree amplitude beyond degree 18 is, in essence, noise on the 5° × 5° grid.

The spectrum at the top of the atmosphere likewise consists of two regions: one in which $\log\sigma_j^2$ decreases somewhat linearly for $j \leq 15$, and one in which $\log\sigma_j^2$ increases somewhat linearly for $j > 15$. This increase in degree variance is a manifestation of the nature of the problem of deconvolution with measurement noise present. It is concluded from Fig. 13 that the coefficients for $j > 15$ are primarily due to noise and contain little information concerning the radiant exitance field. A 15th degree field corresponds to a horizontal resolution of ~1300 km, which is somewhat greater than the satellite altitude of 1100 km. This is in accord with the rule of thumb in a mathematically related problem that the length of the smallest gravitational field feature which can be resolved by observing spacecraft motion equals the spacecraft altitude. Note that gravity fields are essentially constant, so that temporal averaging can be used to continuously reduce effective measurement error, whereas natural variability of the radiative flux limits the accuracy of results derived over the averaging interval.

A map of emitted radiant exitance based on WFOV measurements deconvolved to the top of the atmosphere for August 1975 is shown in Fig. 14. This map is for a degree 15 solution. For the sampling provided by the Nimbus 6 orbit, this is the maximum resolution obtainable as discussed above. Examination of the map shows a number of aspects which can be related to geographic or meteorological features. The major characteristic of the distribution is the latitudinal variation, which has long been recognized (Vonder Haar and Suomi, 1971). There is a band of locally high, radiant exitance areas around the northern and southern subtropical latitudes, corresponding to the subsidences occurring at those latitudes. This map may be compared with maps of longwave radiation for August 1975 computed using Nimbus 6 ERB scanning and WFOV radiometers by Smith *et al.* (1977). Fig. 14 has considerably more detail than does the WFOV map by Smith *et al.*, as is to be expected for a resolution enhancement process. The large scale features are similar. It is noted that the longwave minima associated with the intertropical convergence zone appear in Fig. 14. Also, the two regions of high longwave radiation, one over the western Sahara and one over the Middle East, are resolved by the present technique and match the scanning channel results of Smith *et al.* (1977). A number of such comparisons can be found between the present results and those of Smith *et al.*

The conventional technique for analyzing wide field-of-view radiometer data is to consider each data point to be a measurement of radiative flux from a uniform sphere to an infinitesimal flat plate. By this assumption, the radiant exitance is given by

$$M(\Theta,\Phi) = m(\Theta,\Phi)\left(\frac{r_e + h}{r_e}\right)^2 \tag{24}$$

which is often called the inverse-square law and disregards the smoothing effect of the sensor. It can be shown by use of Eqs. (3) and (13) that for a flat

plate type radiometer [i.e., one for which $g(\alpha) = \cos\alpha$]

$$\lambda_0 = \left(\frac{r_e}{r_e + h}\right)^2. \tag{25}$$

This agrees with the fact that λ_0 is the ratio of the average measurement, or radiant exitance through a sphere at spacecraft altitude, to the average radiant exitance at the top of the earth-atmosphere system. It may be seen from Eq. (15) that if one replaces all λ_j by λ_0, Eq. (17) reduces in essence to Eq. (24). Thus, the conventional technique for analysis of WFOV radiometer data recovers the global average radiant exitance, but all other terms in the series of Eq. (14) remain attenuated by the measurement. In the present technique, all terms are recovered out to the limit of resolution.

5. Conclusions

A deconvolution analysis has been presented for computing the radiant exitance emitted from the top of the atmosphere in terms of wide field-of-view satellite measurements. This analysis provides radiant exitance information at a finer resolution than the field of view of the sensor. However, it is shown that as resolution of the desired radiant exitance increases, the effect of measurement errors increases, limiting the resolution which can be obtained.

The sensitivity of the resulting radiant exitance to errors in the directional model is examined. It is shown that these errors are a function of wavenumber, or fineness of resolution. A flat plate has low sensitivity to directional model errors at low wave numbers, but is sensitive at high wave numbers. The flat-plate sensor reproduces the global average, independent of the directional model. Spherical and restricted field-of-view radiometers are also studied in this manner.

The analysis was applied to Nimbus 6 ERB wide-field-of-view radiometer data for August 1975. It was found that information is present in the measurements out to the 15th degree, corresponding to 1300 km resolution. For the sampling of the Nimbus 6 orbit, this appears to be the maximum resolution obtainable. Comparison of these results with ERB scanning radiometer data shows good agreement.

The spherical harmonic coefficients which are computed during the deconvolution provide a useful representation of the emitted flux density field. It was found that for degrees 0–4, the zonal terms predominate. The degree variance of the radiant exitance field was found to decrease approximately exponentially with wave number from degree 3 out to degree 15.

Acknowledgment. The authors are grateful to Dr. H. Jacobowitz and other members of the Meteorological Satellite Laboratory of NOAA for providing us with ERB data and for discussions with respect to the data.

APPENDIX A

Eigenfunctions of Measurement Operator

In this appendix, it will be demonstrated that the eigenfunctions of the measurement operator $\mathcal{L}$ of Eq. (11) are spherical harmonics, and the formula for the eigenvalues will be derived.

It is noted that the domain of the operator is the set of functions integrable on a sphere, and that the operator is independent of the point on the sphere at which it is applied; i.e., the operator is invariant with respect to rotations in Θ_s and Φ_s. Also, the operator is invariant with respect to rotations about the nadir line through the sensor. With this degree of spherical symmetry, one is assured that the eigenfunctions of the operator are spherical harmonics, which constitute the rotation group.

In addition to the geocentric spherical coordinate system Θ, Φ, a second geocentric spherical coordinate system γ, β is defined as shown in Fig. A1. In this system, the colatitude γ of a point E is the geocentric angle between E and the satellite S. The longitude β of E is the angle NTE in this spherical triangle. The $Y_j^n(\Theta,\Phi)$ can be written in the rotated coordinate system as (Kahan, 1965; Merzbacher, 1961)

$$Y_j^n(\Theta,\Phi) = \sum_{m=-j}^{j} Y_j^m(\gamma,\beta) D_{mn}^j. \tag{A1}$$

The D^j are rotation matrices for spherical harmonics, and have $2j + 1$ columns. These matrices are functions of the rotation, which is defined in terms of Euler angles as follows. Rotate about the z axis through an angle Φ_s to a new system x_1, y_1, z_1 and then about the y_1 axis through angle Θ_s to the system x', y', z'. In the present problem, rotation through the third Euler angle is not required. The

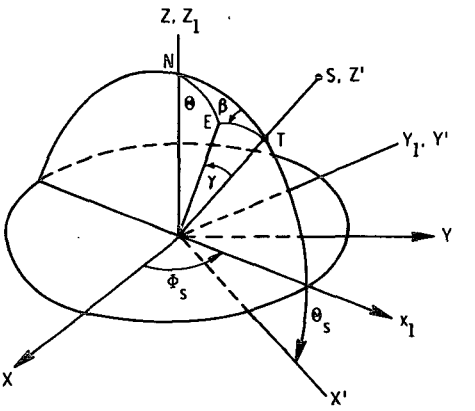

FIG. A1. Rotation from earth-fixed coordinate system to satellite-oriented geocentric coordinate system.

elements of the D^j matrices may be written as (Kahan, 1965)

$$D^j_{mn} = e^{-im\Phi_s} d^j_{mn}(\Theta_s), \tag{A2}$$

where

$$d^j_{mn}(\Theta_s) = \sum_{k\in K} (-1)^k \frac{[(j+n)!(j-n)!(j+m)!(j-m)!]^{1/2}}{(j+m-k)!(j-n-k)!(n-m+k)!k!} \times (\cos\tfrac{1}{2}\Theta_s)^{2j+m-n-2k}(\sin\tfrac{1}{2}\Theta_s)^{n-m+2k}. \tag{A3}$$

The summation is carried out over the set K of all integer values of k for which the factorials in the denominator are non-negative.

With the use of Eq. (A1), $Y^n_j(\Theta,\Phi)$ can be written in the coordinate system most suited to the expression of the operator $\mathcal{L}$. Thus

$$\mathcal{L}Y^n_j(\Theta,\Phi) = \sum_{m=-j}^{j} D^j_{mn}(\Theta_s,\Phi_s)\mathcal{L}Y^m_j(\gamma,\beta) = \sum_{m=-j}^{j} D^j_{mn}(\Theta_s,\Phi_s)\pi^{-1}\int_{\beta=0}^{\beta=2\pi}\int_{\alpha=0}^{\alpha=\alpha_h} Y^m_j(\gamma,\beta) \times R(\theta)g(\alpha)\sin\alpha d\alpha d\beta. \tag{A4}$$

Note that the D^j matrices are constants with respect to the operator $\mathcal{L}$, so that $\mathcal{L}$ and D commute. Also,

$$\pi^{-1}\int_{\beta=0}^{\beta=2\pi}\int_{\alpha=0}^{\alpha=\alpha_h} Y^m_j(\gamma,\beta)R(\theta)g(\alpha)\sin\alpha d\alpha d\beta = \begin{cases} 0, & m \neq 0, \\ \dfrac{(2j+1)^{1/2}}{4\pi}\lambda_j, & m = 0, \end{cases} \tag{A5}$$

where

$$\lambda_j = 2\int_0^{\alpha_h} P_j(\cos\gamma)R(\theta)g(\alpha)\sin\alpha d\alpha \tag{A6}$$

and $P_j(\ )$ denotes the Legendre polynomial of degree j. Eq. (A5) reduces Eq. (A4) to

$$\mathcal{L}Y^n_j(\Theta,\Phi) = D^j_{0n}(\Theta_s,\Phi_s)\frac{(2j+1)^{1/2}}{4\pi}\lambda_j \tag{A7}$$

The right-hand side of Eq. (A7) reduces to spherical harmonics (Kahan, 1965) giving the result that

$$\mathcal{L}Y^n_j = \lambda_j Y^n_j. \tag{A8}$$

Eq. (A8) states that when a radiation field which is distributed as a spherical harmonic is observed, the observation is itself a spherical harmonic. That is, the observation is distributed precisely as the field, differing only by a constant factor λ_j.

APPENDIX B

Comparison with Fourier Integral

It is useful to compare the present problem on the sphere with the corresponding problem on the real line, which is appropriate to signal processing and imaging systems (Katzberg *et al.*, 1973). The corresponding aspects of these two types of problems are listed in Table 1 for comparison. For simplicity, the problem on the sphere will be restricted to the axisymmetric case, for which the physical domain is the colatitude Θ. For signal processing problems, the physical domain is typically time t, which is assumed to be unbounded. As a consequence, the resolution of an arbitrary signal $a(t)$ requires a continuum of waves (of the form $e^{i\omega t}$) of frequencies ω, requiring an integration for their superposition:

$$a(t) = \int_{-\infty}^{\infty} A(\omega)e^{i\omega t}d\omega.$$

Because a sphere is a compact space, an arbitrary axisymmetric distribution on a sphere can be expressed in terms of waves [of the form $P_n(x)$, where $x = \cos\Theta$] with discrete values of n, which are superposed by an infinite summation:

$$a(x) = \sum_{n=0}^{\infty} A_n P_n(x).$$

The measurement $b(t)$ made by a time-independent system may be expressed as a convolution of the signal:

$$b(t) = \int_{-\infty}^{\infty} h(\gamma)a(\tau)d\tau$$

where $\gamma = t - \tau$ is the displacement in time of the measurement from the signal. For a measurement $b(\Theta_s)$ made on a sphere by a position independent system of the type considered in the present paper, the appropriate expression may be written as

$$b(\Theta_s) = \int_{4\pi} h(\gamma)a(\Theta)d\Omega$$

where γ is the geocentric angular displacement of the measurement from the element of the earth's surface subtending the geocentric solid angle $d\Omega$. For a problem on a line, the Fourier transform of the response function $h(\gamma)$ is the transfer function $H(\omega)$;

TABLE 1. Comparison of line and sphere problems.

Item	Line	Sphere
Physical domain	t $(-\infty, \infty)$	Θ ($x = \cos\Theta$) $[0, \pi]$
Type of space	unbounded	compact
Transform variable	ω continuous	n discrete
Transform equation	$A(\omega) = 1/(2\pi) \int_{-\infty}^{\infty} a(t)e^{i\omega t}dt$	$A_n = \frac{1}{2}(2n + 1) \int_{-1}^{1} a(x)P_n(x)dx$
Inverse transform equation	$a(t) = \int_{-\infty}^{\infty} A(\omega)e^{i\omega t}d\omega$	$a(x) = \sum_{n=0}^{\infty} A_n P_n(x)$
Eigenfunctions	$e^{i\omega t}$	$P_n(x)$
Measurement	$b(t) = \int_{-\infty}^{\infty} h(t - \tau)a(\tau)d\tau$	$b(\theta') = \int_{4\pi} h(\gamma)a(x)d\Omega$
Transfer function, eigenvalue	$H(\omega) = \int_{-\infty}^{\infty} h(\tau)e^{i\omega\tau}d\tau$	$\lambda_n = \int_{-1}^{1} h(\gamma)P_n(x)dx$
Measurement wave content	$B(\omega) = H(\omega)A(\omega)$	$B_n = \lambda_n A_n$

this is the ratio of the output of the system to the input for a wave of frequency ω. That is, $\int_{-\infty}^{\infty} h(t - \tau)(\ )d\tau$ is an operator with eigenfunctions $e^{i\omega t}$ and a continuum of eigenvalues $H(\omega)$. For a problem on a sphere, the present paper has demonstrated that if the measurement operator is rotationally invariant, the eigenfunctions are spherical harmonics, which reduce to Legendre polynomials $P_n(x)$ for the axisymmetric case. That is, the output of the system when viewing a wave of order n is a wave of order n and the ratio of output to input is the eigenvalue λ_n, corresponding to the transfer function $H(\omega)$ on the line.

It is thus seen that the mathematical structure of the analysis of wide-field-of-view radiometer data is very similar to that of image processing or of a time-invariant linear dynamical system.

REFERENCES

Bess, T. D., R. N. Green and G. L. Smith, 1981: Deconvolution of wide field-of-view radiometer measurements of earth emitted radiation. Part II: Analysis of first year of Nimbus 6 ERB data. *J. Atmos. Sci.*, **38**, 474–488.

Heiskanen, W. A., and H. Moritz, 1967: *Physical Geodesy*. W. H. Freeman and Co.

Jacobowitz, H., W. L. Smith, H. B. Howell, F. W. Nagle and J. R. Hickey, 1979: The first 18 months of planetary radiation budget measurements from the Nimbus 6 ERB experiment. *J. Atmos. Sci.*, **36**, 501–507.

Kahan, T., 1965: *Theory of Groups in Classical and Quantum Physics*, Vol. I. Oliver and Boyd, Ltd., 566 pp.

Katzberg, S. J., F. O. Huck and S. D. Wall, 1973: Photosensor aperture shaping to reduce aliasing in optical-mechanical line-scan imaging systems. *Appl. Opt.*, **12**, 1054–1060.

Merzbacher, E., 1961: *Quantum Mechanics*. Wiley, 544 pp.

Rapp, R. H., 1977: The relationship between mean anomaly block sizes and spherical harmonic representations. *J. Geophys. Res.*, **82**, 5360–5364.

Raschke, E., T. H. Vonder Haar, W. R. Bandeen and M. Pasternak, 1973: The annual radiation balance of the earth-atmosphere system during 1969–1970 from Nimbus 3 measurements. *J. Atmos. Sci.*, **30**, 341–364.

Smith, W. L., J. Hickey, H. B. Howell, H. Jacobowitz, D. T. Hilleary and A. J. Drummond, 1977: Nimbus 6 earth radiation budget experiment. *Appl. Opt.*, **16**, 306–318.

Suomi, V. E., 1960: Radiation measurement of the earth from an artificial satellite. *Rockets and Satellites in IGY*, Pergamon.

Twomey, S., 1965: The application of numerical filtering to the solution of integral equations encountered in indirect sensing measurements. *J. Franklin Inst.*, **279**, 95–109.

——, 1977: *Introduction to the Mathematics of Inversion in Remote Sensing and Indirect Measurements*. Elsevier, 243 pp.

Vonder Haar, T., and V. Suomi, 1971: Measurements of the earth's radiation budget from satellites during a 5-year period. Part I: Extended time and space means. *J. Atmos. Sci.*, **28**, 305–314.